Hindawi
Advances in Materials Science and Engineering
Volume 2020, Article ID 5072534, 19 pages
https://doi.org/10.1155/2020/5072534

Research Article

Effect of High Temperature (600°C) on Mechanical Properties, Mineral Composition, and Microfracture Characteristics of Sandstone

Jian Li,[1,2] **Zhao-Wen Du**,[1] **and Zhong-Ping Guo**[1]

[1]*College of Energy and Mining Engineering, Shandong University of Science and Technology, Qingdao 266590, China*
[2]*College of Mining and Civil Engineering, Liupanshui Normal University, Liupanshui 553004, China*

Correspondence should be addressed to Jian Li; skdlijian2017@sdust.edu.cn, Zhao-Wen Du; QDDZW3215@sdust.edu.cn, and Zhong-Ping Guo; gzp57046@sdust.edu.cn

Received 28 May 2020; Revised 6 July 2020; Accepted 7 July 2020; Published 12 August 2020

Academic Editor: Fernando Lusquiños

Rock destruction under high-temperature conditions is a key issue for nuclear waste treatment projects, underground coal gasification, and improvement of the use of geothermal energy for heating. Therefore, in this study, various methods and techniques were integrated to study the changes in mechanical properties, mineral composition, and microscopic fracture characteristics of Sichuan sandstone treated at 600°C. First, the fracture toughness and indirect tensile strength of untreated sandstones and high-temperature treated sandstones were tested by the MTS testing machine, and the double-K model (DKFM) was used to estimate the unstable fracture toughness. Then, the diffraction spectra of sandstone were analyzed with an X-ray diffractometer to determine the mineral composition change after heat treatment. Finally, the microscopic features of sandstone were observed through a scanning electron microscope (SEM) and optical microscope. The results show the following. (1) There is no significant change in the tensile strength and fracture toughness of Sichuan sandstone treated at 600°C. (2) The brittleness of Sichuan sandstone decreases and the ductility increases after high-temperature treatment. (3) The unstable fracture toughness value K_{un} obtained by the double-K model (DKFM) is significantly larger than the apparent fracture toughness value K_{if}. (4) After treatment at 600°C, the clay minerals in the sandstone changed significantly. Kaolinite is dehydroxylated to metakaolinite, which may increase the ductility of the rock.

1. Introduction

Increased demand for clean energy has promoted the rapid development of nuclear waste storage [1], geothermal energy and deep resource extraction, and underground coal gasification (UCG) [2]. The design and safety of these projects need to consider the influence of high temperatures on the physical and mechanical properties of rocks, which has thus aroused an interest in the study of the mechanical behavior of rock under high temperature by scholars. Many experimental studies have been conducted on the physical and mechanical properties of rocks under high-temperature conditions, and many important results have been achieved.

Gautam et al. [3] performed tests on Dholpur sandstone and found that the uniaxial compressive strength of sandstone showed a small change within 250°C, increased from 250°C to 650°C, and then began to decline after exceeding 650°C. Zhang et al. [4] conducted experiments on marble, limestone, and sandstone in the range of 20–800°C and found that the mechanical properties of various rocks vary greatly. The peak strength of marble gradually decreased above 400°C, while the strength of sandstone increased from room temperature to 600°C and decreased rapidly after treatment at 600°C. Liu and Xu [5] measured the physical and mechanical properties of granite and sandstone specimens after high-temperature treatment. Their results showed that the compressive strength of granite specimens decreased with increasing temperature, while the compressive strength of sandstone did not show a significant change between room temperature and 800°C but began to decline rapidly above 800°C. Yang et al. [6] tested granite in the range of room temperature to 800°C and found that the

strength and static modulus of elasticity increased from room temperature to 300°C, peaked at 300°C, and began to decline thereafter. Ranjith et al. [7] tested high-temperature-treated Hawkesbury sandstone, and their results showed that the compressive strength and elastic modulus of the sandstone increased with an increase of temperature when the temperature was lower than 500°C. After 500°C, it began to decrease. At the same time, the X-ray diffraction results of sandstone 25 and 950 were compared, which indicated that the mineralogy of sandstone cement had changed obviously and that the kaolinite dehydroxylation reaction occurred at high temperatures. Figure 1 summarizes some of the existing experimental results of uniaxial compressive strength testing of rocks after high-temperature treatment [8, 9]. The results show that the strength of granite decreased significantly when exposed to temperatures near 600°C, compared with that at room temperature, while the strength of most sandstone did not decrease significantly (or even increase significantly). This indicates that the macroscopic mechanical properties of different types of rocks respond differently to high temperatures [10], mainly because the macroperformance of rocks has a significant relationship with mineral composition, grain size, and microstructure. Sandstone is rich in clay minerals, and the changes of clay minerals during high-temperature treatment significantly affect the physical and mechanical properties of the rock; however, the current research into this topic is not sufficient [7].

Fracture toughness is an important indicator for measuring fractures. It describes the resistance of materials to crack propagation [11], and so, many scholars have conducted a large number of experimental studies on the fracture toughness of heat-damaged rocks.

Kuruppu and Seto [12] found that the fracture toughness of Kimachi sandstone increased slightly as the temperature increased to 200°C. The experiment of Nasseri et al. [13] showed that the fracture toughness of Westerly granite decreased by more than 90% from room temperature to 800°C. Feng et al. [14] found that the fracture toughness of sandstone has a clear temperature threshold (500–600°C). When the temperature exceeds this threshold, the fracture toughness drops sharply. Below this threshold, the fracture toughness slowly decreases. Talukdar et al. [15] studied the effects of heat treatment on the fracture toughness (FT) of three crystalline rocks, and the results showed that, from room temperature to 600°C, the FT values of basalt, giant plagioclase basalt, and alstonite decreased by nearly 52%, 68%, and 64%, respectively. They observed that the microcrack density increased with the increase of temperature. Yin et al. [16] demonstrated that the fracture toughness of granite decreases significantly with increasing temperature and number of cycles, while the porosity of the granite increases significantly. Rong et al. [17] experimentally confirmed that thermal damage has important effects on rock strength and deformation behavior. Zuo et al. [1] conducted fracture tests on Beishan granite and found that, in the range of 125–600°C, the fracture toughness of Beishan granite decreased linearly with the pretreatment temperature. Miao et al. [18] believed that the thermally induced

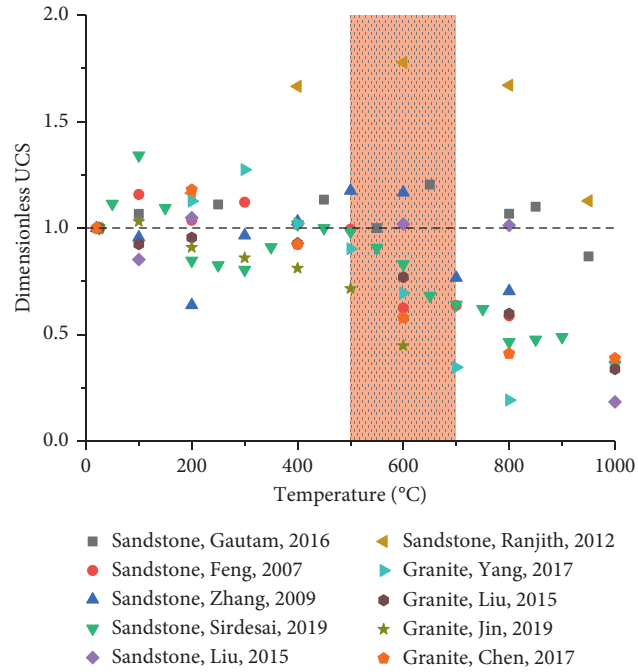

Figure 1: The relationship between normalized uniaxial compressive strength (UCS) and test temperatures, as reported in the literature.

microcracks were an important reason for the change in the fracture behavior of Beishan granite and pointed out that, for granite specimens with a temperature above 300°C, there was a large fracture process zone (FPZ) before the notched tip of the specimen; therefore, linear elastic fracture mechanics (LEFM) are not applicable in this case. Maruvanchery and Kim [19] used a CCNBD specimen to test the fracture toughness of sandstone. It was found that the fracture toughness value of the sandstone after high-temperature (500°C) treatment was significantly reduced, compared to that at low temperature (105°C).

It is worth noting that most rock fracture toughness results have directly applied linear elastic fracture mechanics (LEFM) [20, 21] without considering the influence of the fracture process zone, and so, the rock fracture toughness could have been underestimated. To solve this problem, many nonlinear fracture mechanics models have been developed, such as the size effect model and the double-K model (DKFM) [21, 25]. These models have been successfully applied to the problem of concrete fractures. However, the use of nonlinear fracture mechanics models in rock mechanics is rare, especially in the study of heat-damaged rocks.

In this study, the Brazilian split test and the fracture toughness test of Semicircular Bend (SCB) specimens are conducted on Sichuan sandstone at room temperature and after high-temperature treatment at 600°C, and the double-K model (DKFM) is used to calculate the unstable fracture toughness value (K_{un}). At the same time, XRD, optical microscopy, scanning electron microscopy (SEM), and other methods are used to study the mineral composition and microstructure of sandstone after high-temperature treatment.

2. Materials and Methods

2.1. Specimen Preparations and Heat Treatment. The sandstone specimens in this study were obtained from Sichuan, China, with uniform particles and no obvious macroheterogeneity, as shown in Figure 2. In order to determine the fracture toughness of sandstone, the Semicircular Bend (SCB) specimen, as recommended by the International Society of Rock Mechanics (ISRM), was used. The SCB specimens were carefully processed, according to the method recommended by ISRM [20]. At the same time, a number of Brazilian disc specimens with a diameter of 50 mm and a thickness of 25 mm were produced according to the ISRM method [22], in order to test the tensile strength. See Table 1 and Figure 2 for specific dimensions and parameters.

All specimens were divided into 2 groups, according to the treatment temperature, that is, a room-temperature group (25°C) and a high-temperature group (600°C). The specimens in the room temperature group were only dried, where moisture was removed in a drying cabinet. In the high-temperature group specimens, heat treatment was carried out in an intelligent muffle furnace. The test heating rate was set at 5°C/min. When the temperature rose to the specified temperature, the specimen was kept at this temperature for 1 h. Then, the power was turned off to stop the heating and the specimen was naturally cooled to room temperature in the muffle furnace [13, 23].

2.2. XRD Analysis. In order to understand the different mineral phases of sandstone in detail and to determine the effect of heat treatment on the composition of sandstone, an XRD diffractometer was used to determine the composition of the rock before and after heating [19]. The scanning range was 2°–50° and the scanning speed was 6°/min.

2.3. Rock Mechanical Properties Test

2.3.1. Fracture Toughness. A hydraulic servo-controlled MTS testing machine was used to test the fracture toughness. In order to avoid dynamic effects, all specimens were loaded in the displacement control mode at the same rate of 0.05 mm/min [20]. During the experiment, the axial load and the axial displacement were automatically recorded every 0.01 s [21]. The schematic diagram of the experimental device is shown in Figure 3(a). At the same time, a high-precision extensometer was used to measure the crack mouth opening displacement (CMOD) of the SCB specimen.

The apparent fracture toughness K_{if} is calculated as

$$\begin{cases} K_{\text{if}} = Y\dfrac{P_{\max}\sqrt{\pi a_0}}{2RB}, \\ Y = -1.297 + 9.516\left(\dfrac{S}{2R}\right) - \left(0.47 + 16.457\left(\dfrac{S}{2R}\right)\right)\alpha + \left(1.071 + 34.401\left(\dfrac{S}{2R}\right)\right)\alpha^2, \\ \alpha_0 = \dfrac{a_0}{R}, \end{cases} \tag{1}$$

where $P_{\max}$ is the peak load, a_0 is the initial crack length, R and B are the radius and thickness of the SCB specimen, respectively, Y is the dimensionless stress intensity factor, and S is the distance between the two supporting cylindrical rollers.

The same S value ($S = 80$ mm) was used in this study for all the SCB specimens and $S/2R = 0.8$.

The unstable fracture toughness K_{un} is calculated as

$$K_{\text{un}} = \frac{P_{\max}\sqrt{\pi a_c}}{2RB}Y, \tag{2}$$

where a_c is the critical effective crack length.

According to the double-K fracture model (DKFM), only the critical effective crack length a_c needs to be substituted for the initial crack length a_0 to calculate the unstable fracture toughness K_{un} [24]. The key issue is to estimate the value of a_c, which can be estimated by the compliance equation, detailed as follows.

Evaluation of the elastic modulus E is as follows.

According to Irwin's relationship [25–27], the expression for elastic modulus can be derived:

$$\begin{cases} B \cdot E \cdot C = V(\alpha), \\ C = \dfrac{\text{CMOD}}{P}, \end{cases} \tag{3}$$

where E is the modulus of elasticity. C is compliance. $V(\alpha)$ is nondimensional compliance. CMOD is the crack mouth opening displacement.

The elastic modulus can be obtained by bringing the initial linear compliance C_e into expression (3):

$$\begin{cases} E = \dfrac{V(\alpha_0)}{BC_e}, \\ C_e = \dfrac{\text{CMOD}_e}{P_e}, \end{cases} \tag{4}$$

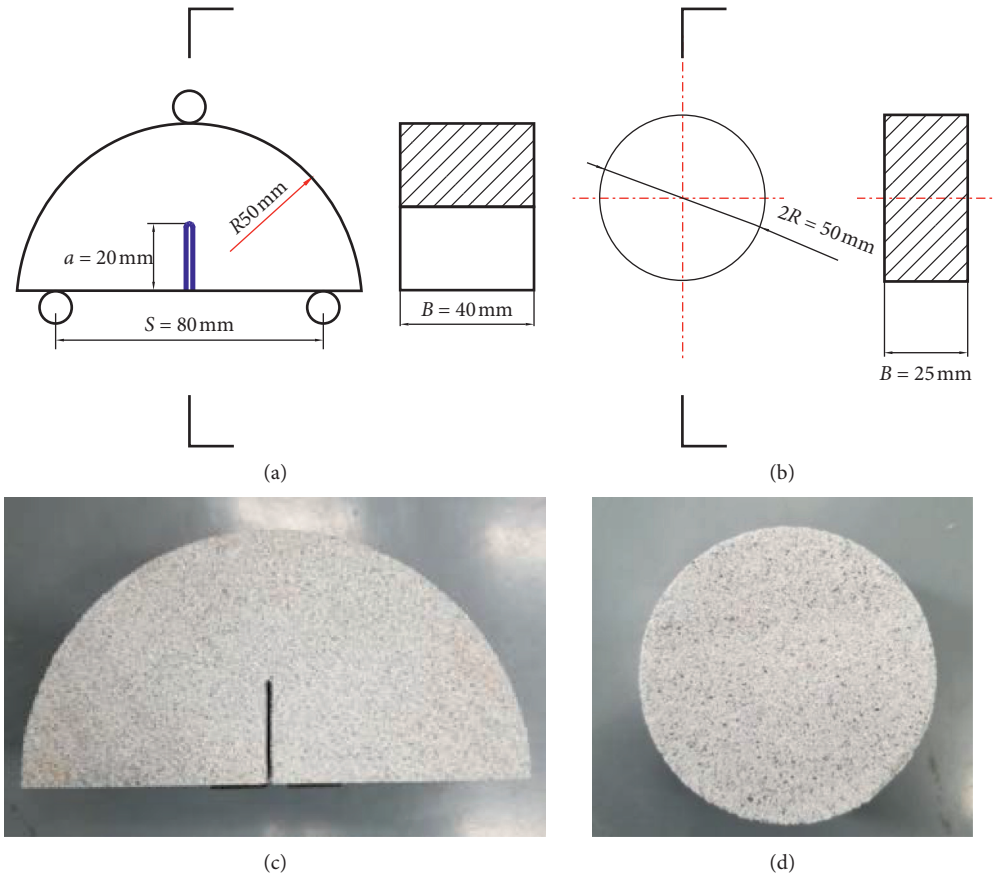

Figure 2: Schematic and real shots of two specimens. (a, c) SCB specimens. (b, d) Brazilian disc specimens (unit: mm).

Table 1: Geometrical dimensions of specimens.

Specimen type	Radius (mm)	Thickness (mm)	Crack length (mm)	Crack length ratio	Number of specimens
SCB	$R = 50$	40	20	0.4	10
BD	$2R = 50$	25	—	-	10

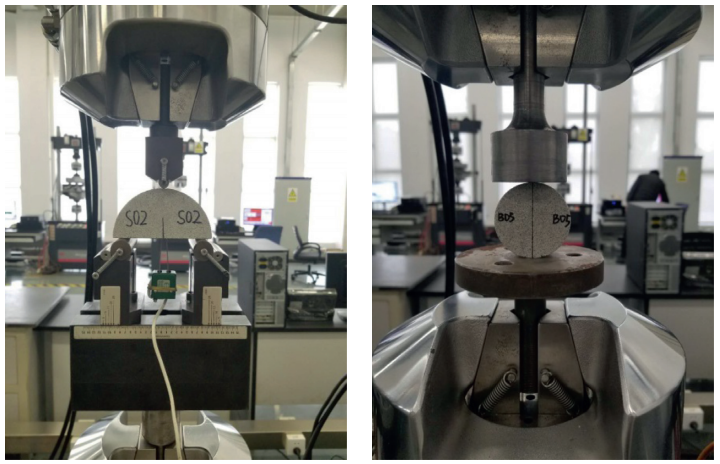

Figure 3: Experimental setup for the fracture toughness test (a) and Brazilian split test (b).

where α_0 is the initial crack length ratio. C_e is the compliance of the initial linear segment of the measured P-CMOD curve.

After the elastic modulus is known, the following expression can be derived according to expression (3):

$$\begin{cases} B \cdot E \cdot C_c = V(\alpha_c), \\ C_c = \dfrac{\mathrm{CMOD}_c}{P_{\max}}, \\ a_c = \alpha_c \cdot R, \end{cases} \tag{5}$$

where CMOD_c is the crack opening displacement at peak load ($P_{\max}$).

The final key issue is to derive the nondimensional compliance $V(\alpha)$. To solve this problem, a finite element program named ABAQUS [28] was used to simulate a set of SCB three-point bending tests ($S/2R = 0.8$), as shown in Figure 4. The results were as follows:

$$\begin{cases} V(\alpha) = 14317.79\,\alpha^6 - 31546.09\alpha^5 + 28013.04\,\alpha^4 - 12470.26\,\alpha^3 + 2924.89\,\alpha^2 - 319.26\,\alpha + 14.09, \\ Y^*(\alpha) = 1231\,\alpha^4 - 2181\,\alpha^3 + 1448\,\alpha^2 - 416.2\,\alpha + 48.29, \\ 0.3 < \alpha < 0.6. \end{cases} \tag{6}$$

To verify the accuracy and effectiveness of the finite element simulation method, Y^* was compared with the dimensionless stress intensity factor Y recommended by ISRM [20], and the results are plotted in Figure 4(b). It can be seen that the difference between Y^* and Y is very small, which indicates that the method is effective and the expression of $V(\alpha)$ is accurate. The accuracy and reliability of the dimensionless stress intensity factor expressions derived by the finite element simulation method have also been confirmed by many studies [29].

After obtaining the expression $V(\alpha)$, the critical effective crack length a_c can be calculated using equation (5), according to the P-CMOD curves obtained from the experiment. $V(\alpha)$ is a higher-order equation, and the critical effective crack length a_c can be calculated using numerical calculation software such as MATLAB. Then, we bring it into equation (2) to calculate K_{un}. Specific details can be found in [21, 24].

2.3.2. Tensile Strength. The tensile strength of the rock is an important parameter. The tensile strength of the specimens before and after heating was measured using the Brazilian disc split method, according to the standard test method provided by the ISRM [22]. The experimental setup is shown in Figure 3(b) and the calculation formula is as follows:

$$\sigma_t = \frac{2P_{\max}}{\pi DB}, \tag{7}$$

where σ_t is the tensile strength of the rock, $P_{\max}$ is the maximum load, D is the diameter of the Brazilian disc, and B is the thickness of the specimen.

2.4. SEM Observation of Microfractures. In order to observe the microscopic morphology and cracks of the fracture, scanning electron microscopy (SEM) was used to observe and compare the changes of the fracture morphology of the rock before and after heating, such as steps and river patterns [30], as well as the clay minerals of sandstone (e.g., kaolinite or green mudstone) [31]. At the same time, in order to understand the effects of temperature on the sandstone minerals, microdomain chemical analysis was performed using Energy Dispersive X-ray Spectroscopy (EDS).

2.5. Optical Microscope. In order to understand the mineral composition and internal structure changes of sandstone after high-temperature treatment, thin slices of sandstone were produced before and after high temperature, which were observed under a polarizing microscope (plane-polarized light and cross-polarized light).

As the thin slices cannot easily distinguish the pore structure in the rock, the sandstone was impregnated with epoxy resin added with blue dye, in order to visually compare the size of the pores and cracks in the sandstone before and after heating. In this way, the blue resin highlighted the pores and cracks, and it was possible to analyze the pores and crack structures intuitively and clearly, as well as to estimate the porosity and other characteristics of the sandstone [32–34].

3. Experimental Results

3.1. Appearance Color Change. The most intuitive effect of heat treatment on Sichuan sandstone was the change of appearance, in terms of color. Comparing the specimens before and after heating, it was found that the surface color of the test piece changed from white-gray to brown-red after heating, as shown in Figure 5.

Color changes have been observed in various rock heating experiments [2, 35–37], and Li et al. [38] even developed a method to determine the degree of rock damage based on the color of the rock. These studies all showed that the color change is related to the trace ferrous metal elements present in the clay minerals in the rock. The presence of elemental Fe was also confirmed by EDS in this experiment, as shown in Figure 6. Even with a very low presence in

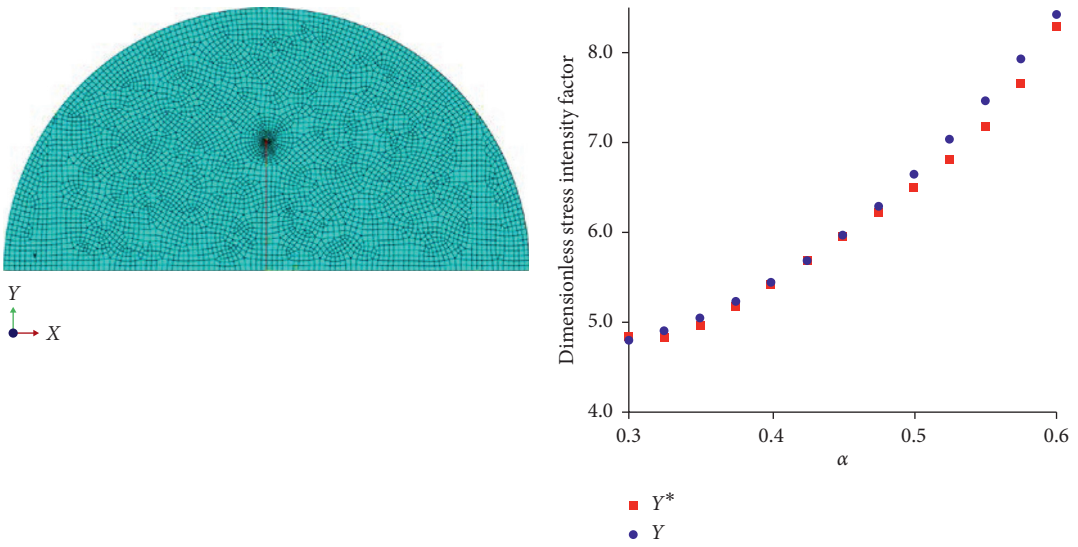

(a) (b)

Figure 4: (a) The model of the SCB specimen in ABAQUS; (b) the values of Y^* and Y.

(a) (b)

Figure 5: The color change of Sichuan sandstone (a) at room temperature and (b) after treatment at 600°C.

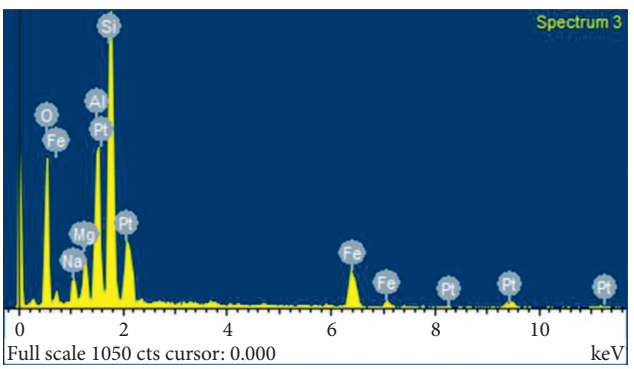

Figure 6: The result of microdomain EDS.

rock, they can have a great impact on the appearance color [37].

3.2. XRD Analysis Results. The mineral composition of sandstone before and after heating was analyzed by X-ray diffractometry. The results are shown in Figure 7 and Table 2. It can be seen that quartz and plagioclase were the main minerals in the sandstone, and the proportions of quartz and plagioclase did not change significantly before and after heating; however, the proportion of clay minerals changed significantly. The total amount of clay minerals decreased from 18.9% before heating to 5.7%. For example, it can be clearly observed from the XRD diffraction patterns (Figure 7) that the diffraction peak of kaolinite in heated sandstone was significantly reduced. This change is mainly due to the removal of hydroxyl groups in the dehydroxylation reaction changing kaolinite to metakaolinite [39], which is in a transition state between crystalline and amorphous and, so, its diffraction peak disappears on the XRD pattern of sandstone after high-temperature treatment. The decarboxylation of kaolinite was also found in the results of the microdomain EDS.

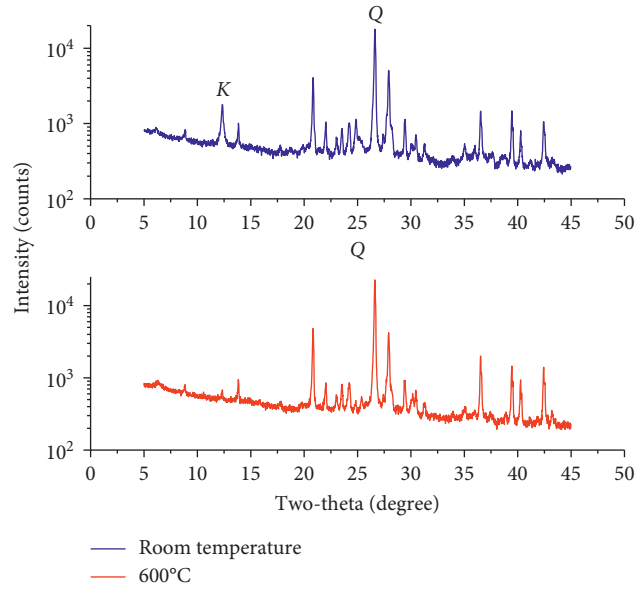

Figure 7: Results of X-ray diffraction and mineral composition (Q: quartz, K: kaolinite; the blue line is at room temperature; the red line is after treatment at 600°C).

3.3. Rock Mechanical Properties Test Results

3.3.1. P-COMD Curves of SCB Specimens. As the P-COMD curve is more sensitive than the load–deflection curve, the effective crack length can be calculated based on this curve [21, 24]. An extensometer was used to record the crack mouth opening displacement (CMOD) in this test, as shown in Figure 8.

The blue curves in Figure 8 are the SCB specimens at room temperature, and the red curves are the SCB specimens after treatment at 600°C. In general, all P-CMOD curves showed a similar trend. That is, the load increased almost linearly in the initial stage (as the CMOD increased). When more than half of the peak load was reached, the linear relationship between the load and CMOD gradually disappeared. The load peaked and then decreased as CMOD increased.

The peak loads and the slopes of the linear phase of P-CMOD curves S01–S05 at room temperature were higher than those after treatment at 600°C: the former curves were higher and thinner than the latter, and the postpeak part of the curves dropped faster.

The average value of the peak load of the SCB specimens at room temperature was $P_{max} = 1307$ N and the average value of the opening displacement of the crack opening at the peak value was CMODc = 0.0875 mm. After treatment at 600°C, the average value of the peak load of the SCB specimens was $P_{max} = 1207$ N and the average value of the crack opening displacement at the peak value was CMODc = 0.146 mm. This shows that sandstone is more ductile after treatment at 600°C than at room temperature. This phenomenon was also observed in the Brazilian split test and is consistent with the test results of Zuo et al. [1], Yin et al. [24], and Miao et al. [18].

Table 2: XRD analysis results.

Rock mineralogy	Weight (%) room temperature	Weight (%) 600°C
Quartz	44.0	46.5
Plagioclase	32.9	31.4
Total clay	18.9	5.7
Calcite	3.3	2.8
Orthoclase	0.9	0.6
Other		13.0

3.3.2. Fracture Toughness. According to the test data of the SCB specimen, the fracture toughness equations (1)–(5) were used to calculate the apparent fracture toughness K_{if} and unstable fracture toughness K_{un}, respectively. The results are shown in Table 3.

It can be seen, from Table 3 and Figure 9, that the average fracture toughness after treatment at 600°C was slightly lower than the average fracture toughness at room temperature, but the change was not large. The average value of the apparent fracture toughness was $K_{if}^{RT} = 0.46$ MPa·m at room temperature, and $K_{if}^{600°C} = 0.42$ MPa·m after heating, a decrease of only 8.69% compared with the original. Similarly, the average value of fracture toughness at room temperature was $K_{un}^{RT} = 0.65$ MPa·m, which became $K_{un}^{600°C} = 0.60$ MPa·m after heating, a decrease of only 8.70% compared with the original. After the sandstone was treated at 600°C, both the apparent fracture toughness K_{if} and the unstable fracture toughness K_{un} showed a slight decrease, but the change was not significant.

However, the unstable fracture toughness value K_{un} was obviously higher than the apparent fracture toughness K_{if}. At room temperature, the K_{un} value of the sandstone was 41.30% higher than that of K_{if}. After heating, the K_{un} value of

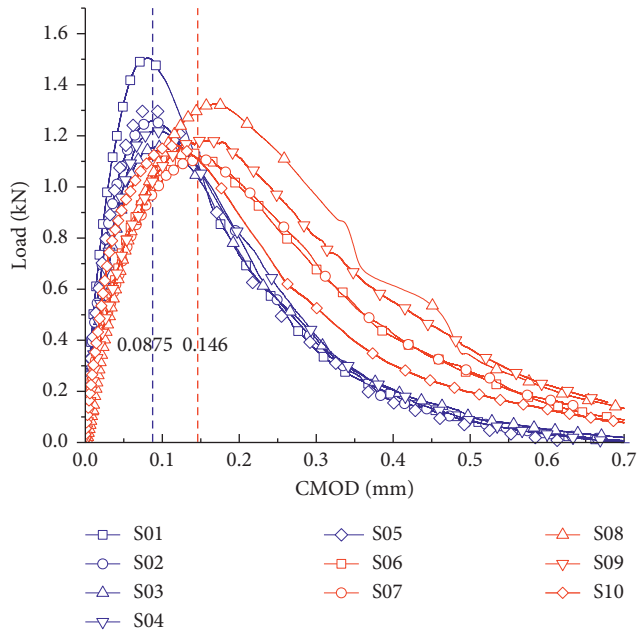

Figure 8: P-CMOD curves. The blue curves indicate the specimen at room temperature, and the red curves indicate the specimen after treatment at 600°C treatment. The vertical dashed line on the graph represents the average critical crack mouth opening displacement (CMODc).

Table 3: The geometrical dimensions and fracture toughness of the specimens.

Specimen no.	R (mm)	B mm)	a_0 (mm)	a_c (mm)	Treatment temperature (°C)	Load P_{max} (N)	$CMOD_c$ (mm)	Elastic modulus (GPa)	K_{if} (MPa•m)	K_{un} (MPa •m)
S01	50.20	40.41	20.15	29.20	Rt	1525	0.0821	11.28	0.52	0.76
S02	50.02	40.10	20.14	28.50	Rt	1276	0.0834	8.81	0.44	0.63
S03	49.98	38.88	21.35	27.32	Rt	1178	0.0944	6.48	0.45	0.58
S04	50.23	39.52	20.35	27.18	Rt	1235	0.0915	6.73	0.43	0.58
S05	49.95	40.72	21.08	29.38	Rt	1323	0.0863	9.59	0.47	0.69
Average						1307	0.0875	8.58	0.46	0.65
S06	49.82	40.54	21.58	27.93	600	1150	0.1333	4.65	0.43	0.57
S07	50.16	40.89	20.13	27.71	600	1134	0.1624	3.56	0.38	0.52
S08	50.16	40.89	20.13	27.92	600	1339	0.1667	4.18	0.45	0.62
S09	50.75	40.77	20.94	29.47	600	1234	0.1528	4.82	0.42	0.61
S10	50.13	40.74	22.01	30.37	600	1178	0.1173	7.02	0.42	0.65
Average						1207	0.146	4.85	0.42	0.60

Note. S, SCB specimen; RT, room temperature (without heat treatment).

the sandstone was also 42.86% higher than that of K_{if}. This indicates that the fracture toughness value directly calculated based on linear elastic fracture mechanics is underestimated. This problem has been noticed, but nonlinear fracture mechanics have not been widely used in the study of rock materials [24].

3.3.3. Load-Displacement Curves of Brazilian Split Test. Figure 10 shows the load-displacement curves obtained from the Brazilian split test. The blue curves are from the specimens at room temperature, and the red curves are from the specimens after treatment at 600°C. It can be observed that there was a significant change after high-temperature treatment. The average peak values of the curves at room temperature and the displacements at the peak value were lower than those after high-temperature treatment. The details are as follows.

The average peak load at room temperature was $P_{max}^{RT} = 5142\,N$ and the average displacement at the peak was $\delta_p^{RT} = 0.2312\,mm$, while the average peak load after treatment at 600°C was $P_{max}^{600°C} = 6257\,N$ and the average displacement at the peak was $\delta_p^{600°C} = 0.4204\,mm$.

It is worth noting that the average peak load of sandstone after treatment at 600°C treatment was higher than that at room temperature, which differs from the fracture toughness test results. This was due to the difference in the fracture form of the two specimens and the heterogeneity of the rock after heating. A more detailed analysis is presented in the Discussion section.

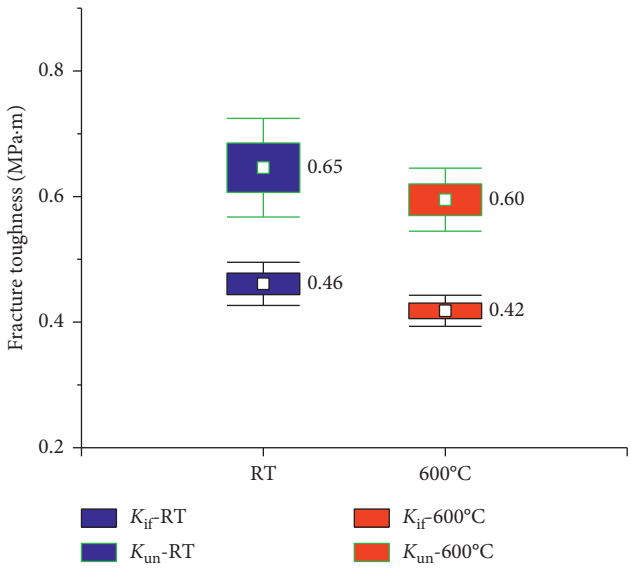

Figure 9: Average fracture toughness (the blue is at room temperature; the red line is after treatment at 600°C).

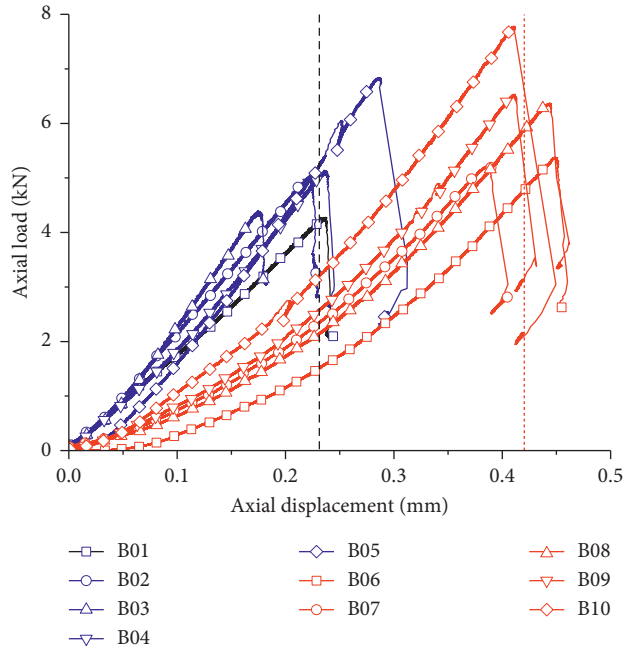

Figure 10: The load-displacement curves of Brazilian split specimens (the blue line is at room temperature; the red line is after treatment at 600°C).

3.3.4. Tensile Strength. According to the Brazilian disc split test data, equation (7) was used to calculate the tensile strength of the sandstone. The results are listed in Table 4 and the average and standard deviation are shown in Figure 11. The tensile strength of sandstone at room temperature was $\sigma_t = 2.64$ MPa; after treatment at 600°C, the tensile strength of sandstone was $\sigma_t = 3.2$ MPa, which was 21.21% higher than that at room temperature.

3.4. Microscopic Analysis of Fracture. The micromorphology of rock fracture is an important part of this test. It truly records the whole process of the fracture, which can reflect the stress of the rock during the fracture process and the characteristics of structural damage to a certain extent. Therefore, a scanning electron microscope (SEM) was used to observe the fracture microtopography features, such as cleavage, steps, and river patterns.

3.4.1. SEM. By sampling the fractures of the specimens after the test and observing them under the scanning electron microscope, it was found that the SEM images after treatment at 600°C (Figures 12(a), 12(c), and 12(e),) were significantly rougher than those that at room temperature (Figures 12(b), 12(d), and 12(f)). Comparing Figures 12(a) and 12(b), it can be seen that the fractures at room temperature were smooth, and the river and step patterns are not obvious, while the river and step patterns after treatment at 600°C are obvious and rougher [30]. Obvious cracks were observed in the SEM images (Figure 12(b)).

At the same time, clay minerals were observed under the scanning electron microscope, such as the book-shaped kaolinite (Figures 12(c) and 12(d)) and needle-shaped chlorite (Figure 12(e)). This was consistent with the XRD results.

After treatment at 600°C, minerals such as book-shaped kaolinite can still be observed in the SEM images (Figure 12(d)). However, through the results of Energy Dispersive X-ray Spectroscopy (EDS), it was found that the proportion of oxygen was significantly reduced, as shown in Figure 13. This was due to the fact that, after treatment at 600°C, the kaolinite was dehydroxylated to become metakaolinite (equation (8)), which is in a transition state between crystalline and amorphous [39] and, so, the diffraction peak of kaolinite disappeared in the XRD pattern. However, this still has the basic morphology of the original kaolinite and could still be observed in the SEM images.

Although there was no significant morphological change, the activity of metakaolinite was obviously enhanced, which may strengthen the binding force between mineral grains and offset the negative effects of heat loss on rock strength. This is consistent with the views of Mahanta et al. [40] and Ranjith et al. [7]:

$$Al_4Si_4O_{10}(OH)_8 \xrightarrow{600^\circ C} 2Al_2Si_2O_7 + 4H_2O \quad (8)$$

3.4.2. Optical Microscopy. Although the resolution of the SEM is high and the detailed three-dimensional morphology of mineral grains can be seen in the SEM image, the mineral particles can only be shown in gray. A polarized light microscope can easily identify common mineral grains and mesostructures through polarized light, with a low cost. In particular, when the casting technology is adopted, the pores and cracks of the rock could be visually observed, and the porosity of the rock can be evaluated. Therefore, in order to fully understand the characteristics of sandstone after high-temperature treatment, thin slices and casting technology

Table 4: Brazil split test results.

Specimen no.	R (mm)	B (mm)	Treatment temperature (°C)	$\delta_{P\max}$ (mm)	Load $P_{\max}$ (N)	σ_t (MPa)
B01	49.66	25.11	RT	0.2370	4278	2.184
B02	49.45	25.24	RT	0.2221	5054	2.578
B03	49.62	25.09	RT	0.1748	4405	2.252
B04	49.45	24.88	RT	0.2355	5142	2.661
B05	49.22	25.02	RT	0.2868	6833	3.532
Average				0.2312	5142	2.641
B06	49.76	24.97	600	0.4485	5379	2.756
B07	49.82	25.15	600	0.3870	5225	2.655
B08	49.74	25.13	600	0.4444	6369	3.244
B09	49.73	24.98	600	0.4115	6535	3.349
B10	49.43	25.22	600	0.4104	7778	3.972
Average				0.4204	6257	3.195

B, Brazilian split specimen; RT, room temperature (without heat treatment).

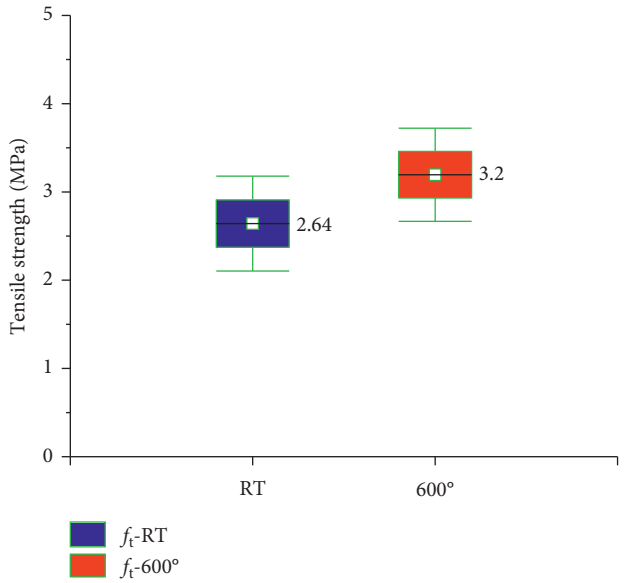

Figure 11: Tensile strength at room temperatures and after treatment at 600°C (the blue is at room temperature; the red line is after treatment at 600°C).

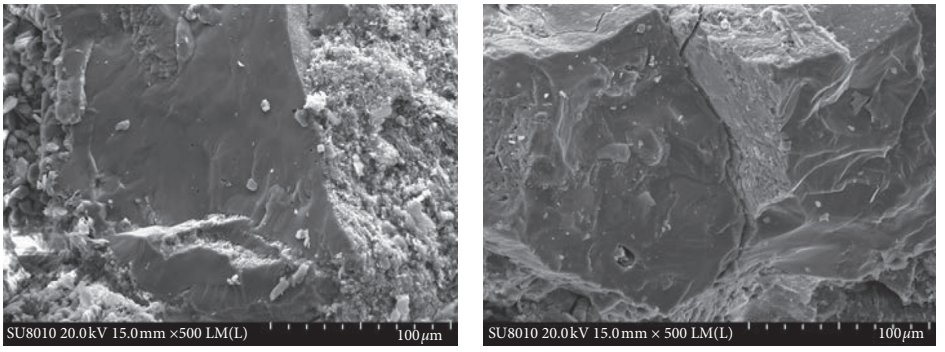

(a) (b)

Figure 12: Continued.

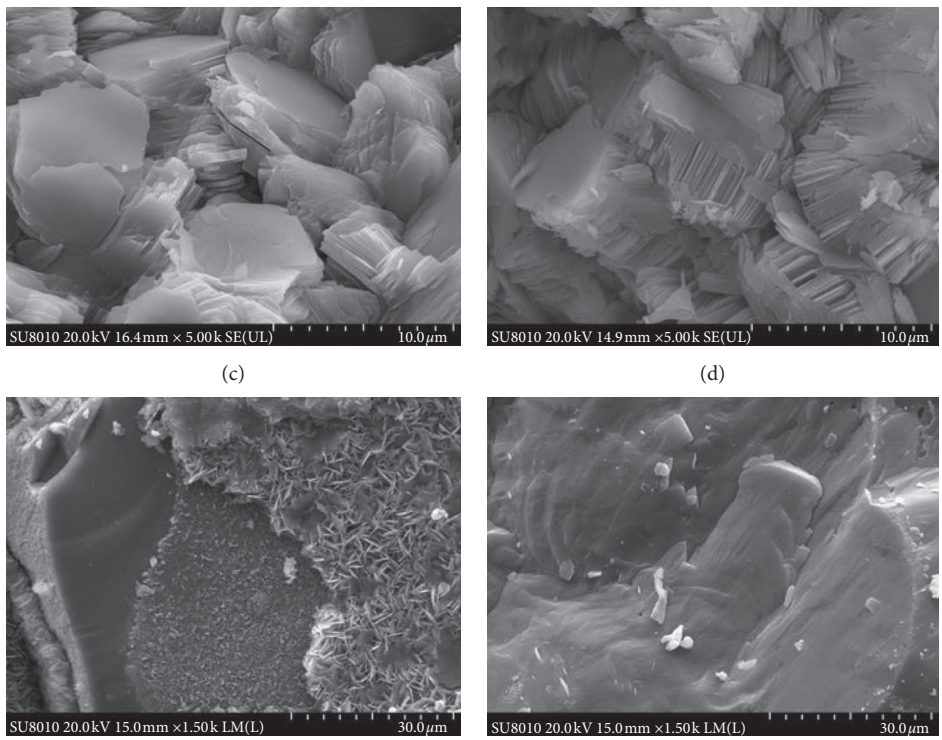

Figure 12: SEM images of fracture: (a, c, e) room temperature; (b, d, f) after treatment at 600°C.

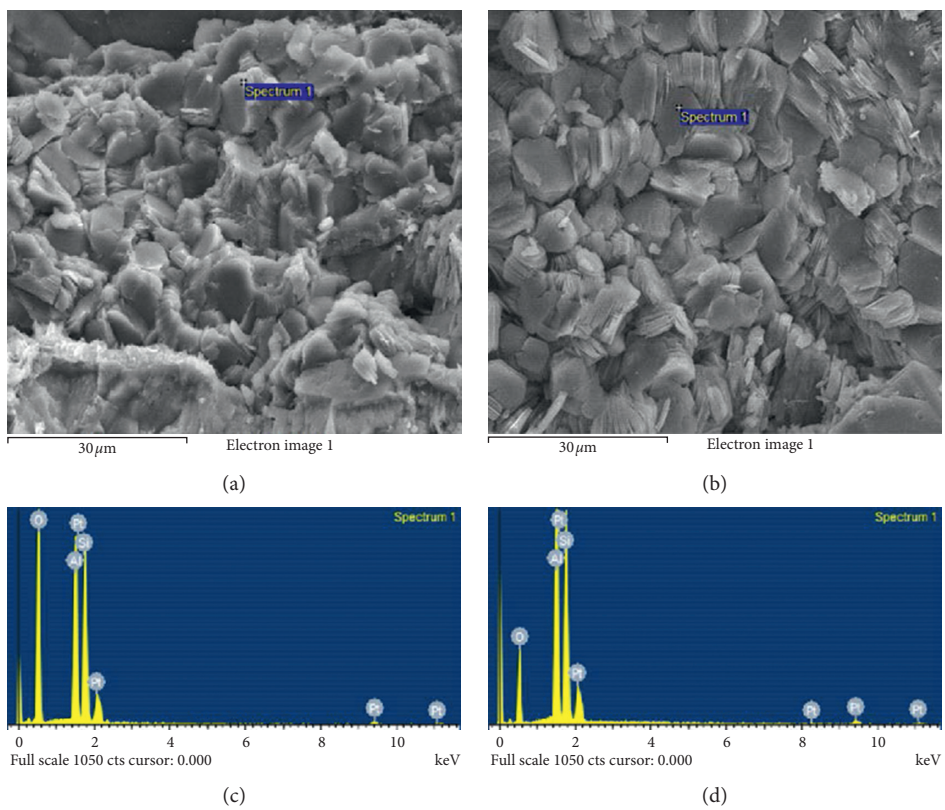

Figure 13: Continued.

Element	Weight %	Atomic %
O K	73.20	82.46
Al K	12.96	8.66
Si K	13.85	8.88
Totals	100.00	

(e)

Element	Weight %	Atomic %
O K	50.02	63.28
Al K	24.04	18.03
Si K	25.94	18.69
Totals	100.00	

(f)

Figure 13: Energy Dispersive X-ray Spectroscopy (EDS) results: (a, c, e) room temperature; (b, d, f) after treatment at 600°C.

were used to observe the change of sandstone characteristics after high-temperature treatment.

Figures 14(a) and 14(c) are thin sections of sandstone at room temperature, and Figures 14(b) and 14(d) are thin sections of sandstone after treatment at 600°C. From the thin section results, it can be seen that the color of the interstitial material between the sandstone mineral grains deepened after treatment at 600°C and changed significantly, which was consistent with the appearance change (Section 3.1). This was related to the changes in clay minerals after high-temperature treatment.

Sandstone samples at room temperature and after high-temperature treatment were impregnated with blue epoxy resin and made into thin slices, as shown in Figure 15. The blue areas are epoxy resin, indicating the pores and cracks in the sandstone. The results of the thin section of sandstone samples at room temperature show that there were not only large pores but also cracks along the grain boundaries of the mineral particles. However, after treatment at 600°C, the proportion of pores and cracks decreased significantly, with almost no significant grain boundary cracks.

This was due to a significant change in the clay minerals between the sandstone mineral grains after high-temperature treatment. For example, the dehydration and dehydroxylation reactions of kaolinite cause the mineral grains to become more closely connected, blocking the tiny channels between the mineral grains. The oxygen resin can only intrude into large pores.

To quantitatively analyze the results of the slices, the ImageJ software was used to analyze the pore structure. The software identified the blue epoxy resin and highlighted it in red, as shown in Figures 15(b) and 15(d). The results show that the surface porosity of sandstone at room temperature was 13.6%, but the surface porosity after high-temperature treatment was only 4.0%.

4. Discussion

The macroscopic mechanical properties of rocks are closely related to the types, sizes, and shapes of mineral grains, as well as the distribution and direction of microcracks [41]. High temperatures can change the microstructure and mineral composition of the rock, and so, the mechanical properties of the rock will change significantly after high-temperature treatment. Different types of rocks have different physical and mechanical properties in response to high temperatures; these differences indicate the complexity of the rocks after heating [42].

4.1. Effect of Temperature on Macromechanical Properties. According to the results of the Brazilian disc split test (Table 4, Figure 11), the average tensile strength of sandstone after 600°C treatment increased slightly than that at room temperature, which seems to contradict the results of fracture toughness. This is due to the increase in the ductility of the sandstone after high-temperature treatment. During the Brazilian split test, after the initial crack was generated, the split sample can still continue to bear the load. Therefore, directly using the peak stress of the Brazilian split test to estimate the tensile strength will cause a deviation. For example, Yin et al. [16, 24] used acoustic emission (AE) to monitor the rock fracture test. It was found that an acoustic emission event suddenly occurred near the peak to the untreated rock. For the rocks after high-temperature treatment, AE activities have been detected prior to peak load, and the cumulative AE counts after the peak continue to increase. This indicates that the high-temperature treated rock cracked before the peak load, so the peak stress may overestimate its tensile strength.

Peng [43] used the discrete element CA2 software to simulate the direct tensile test of rock. In order to independently study the effect of ductility on the mechanical properties of rock materials, other parameters were kept unchanged in the experiment. Only we decrease the Knp value (constitutive parameter, strain-softening slope after peak value, the larger the value, the smaller the ductility) to increase the ductility of the rock. It is indicated that the peak stress increases with ductility while the maximum strength of the linear elastic part showed little variation. The maximum strength of the linear elastic part may reflect the true tensile strength, so the true tensile strength does not increase significantly with ductility.

In the Brazilian split test, we also believe that the contact angle a of the disk specimen and the loading block has an important influence on the test results. Due to the increased ductility of the sandstone after high-temperature treatment, the peak strain and axial displacement increase, so the contact angle a of the sandstone after high-temperature treatment is greater than room temperature, that is, $\alpha^{600^\circ C} > \alpha^{RT}$. According to the results of García et al. [44] and Komurlu et al. [45] on the Brazilian split, the tensile strength should be corrected using the correction factor $ß$. The details are as follows:

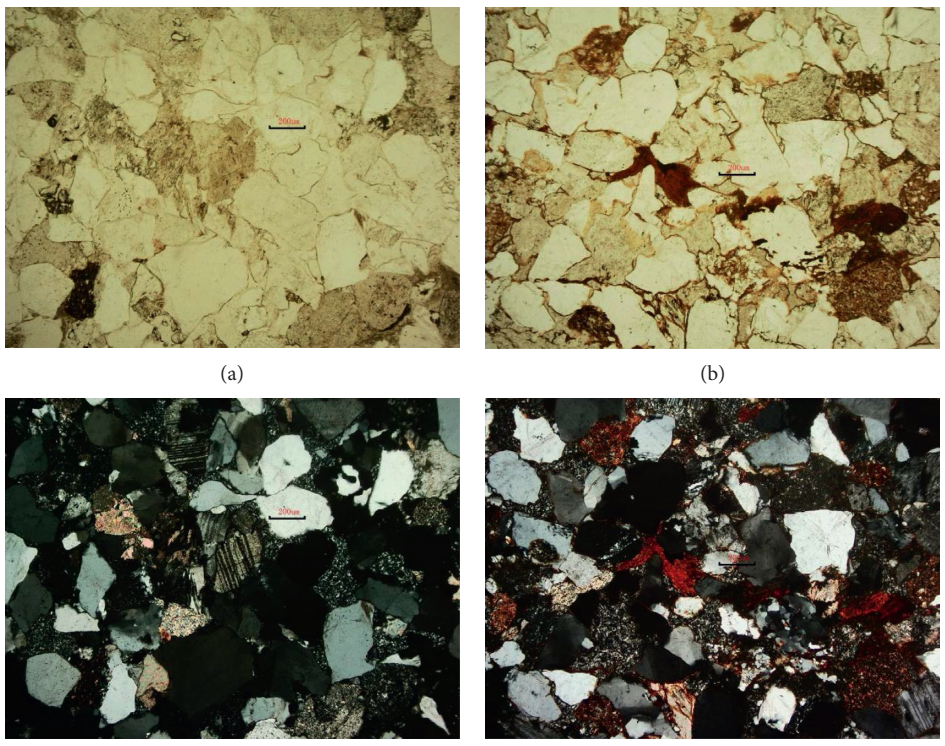

(a) (b)

(c) (d)

Figure 14: Photomicrographs of thin sections of sandstone: (a, b) plane-polarized light; (c, d) cross-polarized light; (a, c) room temperature; (b, d) after treatment at 600°C.

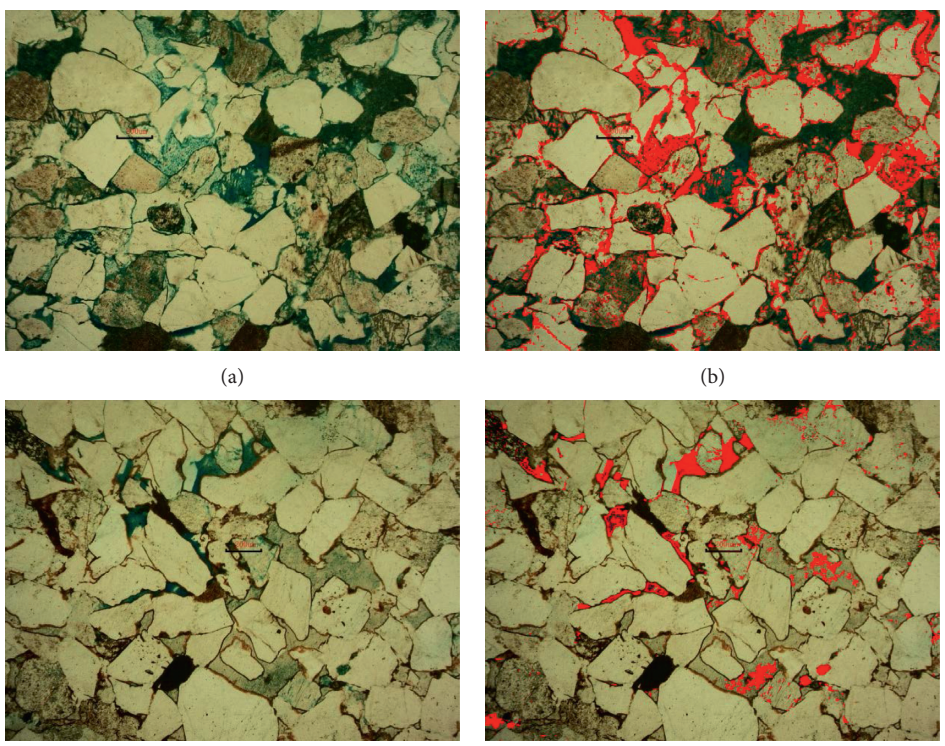

(a) (b)

(c) (d)

Figure 15: Photos of casting thin sections: (a, b) room temperature; (c, d) after treatment at 600°C. The red areas in panels (b) and (d) are the holes and cracks identified by ImageJ software corresponding to panels (a) and (c), respectively.

$$\begin{cases} \sigma_t = \dfrac{2P_{\max}}{\pi \quad Dt}\beta, \\ \\ \beta = \dfrac{\sin\alpha\cos 2\alpha}{\alpha}. \end{cases} \tag{9}$$

According to Expression (9), $\beta^{600^\circ C} > \beta^{RT}$, as shown in Figure 16.

The relative increase $\Delta\sigma_t$ in tensile strength of sandstone after high-temperature treatment without considering the correction factor β is

$$\Delta\sigma_t = \frac{\sigma_t^{600^\circ C} - \sigma_t^{RT}}{\sigma_t^{RT}}. \tag{10}$$

The relative increase Δf_t in tensile strength after taking into account the correction factor β is

$$\Delta f_t = \frac{\beta^{600^\circ C}\sigma_t^{600^\circ C} - \beta^{RT}\sigma_t^{RT}}{\beta^{RT}\sigma_t^{RT}}. \tag{11}$$

According to equations (10) and (11), the following expression (12) can be further obtained:

$$\Delta f_t = \frac{\left(\beta^{600^\circ C}/\beta^{RT}\right)\sigma_t^{600^\circ C} - \sigma_t^{RT}}{\sigma_t^{RT}} < \frac{\sigma_t^{600^\circ C} - \sigma_t^{RT}}{\sigma_t^{RT}} = \Delta\sigma_t. \tag{12}$$

Since the contact angle a of sandstone after high-temperature treatment increases, the difference in tensile strength increase without considering the correction factor (ISRM formula) will be overestimated, that is, $\Delta f_t < \Delta\sigma_t$.

In summary, we believe that the change in the true tensile strength of sandstone after high-temperature treatment is not as significant as the original. This is similar to the test results of fracture toughness. This is also consistent with the law of a positive correlation between tensile strength and fracture toughness [15, 46, 47].

Although the tensile strength and fracture toughness of the sandstone after 600°C treatment did not change significantly, the average elastic modulus decreased from 8.58 Gpa to 4.85 Gpa (Table 3), which indicates an increase in the ductility of the sandstone.

4.2. From Brittleness to Ductility. Rock brittleness can be quantitatively analyzed based on stress-strain curves; unconfined compressive strength and Brazilian tensile strength; mineral composition, porosity, and grain size; and geophysical methods (Zhang et al. [48]). Here, the stress-strain curve is used to quantify the brittleness index (BI); the specific expression is as follows:

$$\mathrm{BI} = \frac{\varepsilon_{el}}{\varepsilon_{tot}}, \tag{13}$$

where ε_{el} is the elastic strain and ε_{tot} is the total strain at failure.

The stress-strain diagram was redrawn according to the results of the Brazilian split test. For ease of analysis, the loading curves of the untreated group and the 600°C treated group were fitted separately, as shown in Figure 17.

According to equation (13), the brittleness index results are as follows:

$$\mathrm{BI}_{RT} = \frac{\varepsilon_{el}^{RT}}{\varepsilon_{tot}^{RT}} = 0.83,$$
$$\mathrm{BI}_{600^\circ C} = \frac{\varepsilon_{el}^{600^\circ C}}{\varepsilon_{tot}^{600^\circ C}} = 0.66. \tag{14}$$

It can be seen that the brittleness index of sandstone after high-temperature treatment is obviously lower than that of untreated sandstone.

In this test, although the treatment at 600°C had no significant effect on the strength of sandstone, it can be clearly seen that the ductility of sandstone increased significantly after high-temperature treatment. The average value of critical crack opening displacement of SCB specimens at room temperature was CMODc = 0.0875 mm. After treatment at high temperature, this value became CMOD_c = 0.146 mm, an increase of 66.86%. Similarly, at room temperature, the average value of the displacement direction of the Brazilian split test of the sandstone in the loading direction was δ_p = 0.2312 mm, which became δ_p = 0.4204 mm after treatment at 600°C, an increase of 81.83% (see Figures 8 and 10).

The increase of CMODc and peak displacement is also one of the characteristics of increased rock ductility. More typical is the change of the P-CMOD curve shape. As shown in Figure 8, the shape of the sandstone P-CMOD curve after high-temperature treatment changes from tall to thin, and the postpeak parts of the curves are significantly different. For untreated sandstone, the postpeak part decreases rapidly, but the postpeak part of the sandstone decreases more slowly after high-temperature treatment. Miao et al. [18] reported that the ductility characteristics of rocks after high-temperature treatment are more obvious, the peak load is reduced, and the critical crack opening displacement is increased (CMODc). Yin et al. [24] stated that as the processing temperature increased, more yield stages appeared in the prepeak stage of the P-CMOD curve, and softening behavior appeared in the postpeak stage and said that this change means that the heat treatment seriously affected the brittleness of the rock. Eventually, the fracture of the rock changed from brittleness to ductility.

Usually, the brittle rock will break quickly when it is loaded to the peak, and the crack propagation speed is fast. For the rock after high-temperature treatment, the ductility increases, the peak strain increases, the loading process becomes longer, and the breaking speed decreases. If acoustic emission monitoring is used, the cumulative AE counts will only increase significantly for brittle rocks near the peak. For high-temperature treated rocks, cumulative AE counts will appear before the peak, and the AE count rate after the peak is higher. For example, Yin et al. [16] reported that the AE event in the postpeak period of the rock after high-temperature treatment is still very active and said that this is a sign of increased ductility.

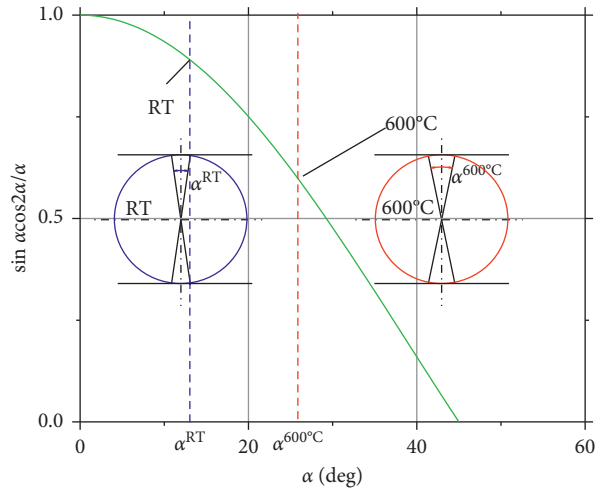

Figure 16: Variation of the correction factor β with a contact angle a (the blue circle and the red circle represent the untreated sandstone and 600°C treated sandstone in the Brazilian split test $\alpha^{600°C} > \alpha^{RT}$).

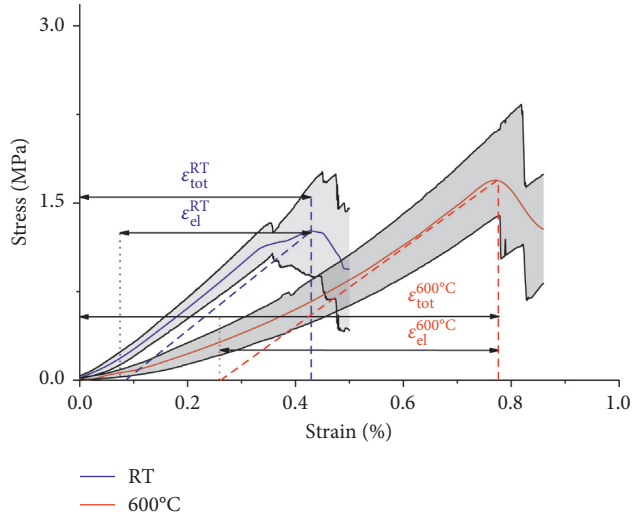

Figure 17: Brazil splitting stress-strain diagram (the loading curve in the figure is the result of fitting multiple Brazilian splitting curves, and the shaded part represents the error band of one standard deviation).

The microanalysis results of fractures indicated that the sandstone became rough after high-temperature treatment, with obvious river and step patterns (see Figure 12). This is consistent with the scanning electron microscopy results of sandstone after high-temperature treatment by Zuo et al. [30]. Both macroscopically and microscopically indicate that the fracture behavior of sandstone after high-temperature treatment reduces brittleness and increases ductility.

4.3. Differences in Mechanical Properties of Different Rocks after High Temperature. The change in the strength of sandstone after high-temperature treatment was very different from the test results in many other crystalline rocks. The strength of most granite has a significant decrease after treatment at 600°C ([1, 5, 6, 13, 23, 49], as Figure 1). Liu et al. [50] compared the experimental results of sandstone and granite after high-temperature treatment and found that the UCS of granite specimens generally decreased with increasing temperature, while the UCS of sandstone specimens did not change significantly from room temperature to 800°C.

As the mineral compositions and microstructures of different types of rocks are significantly different, the mechanical properties of different types of rocks after high-temperature treatment are significantly different.

Sandstone is a sedimentary rock, in which there are many cementing elements between mineral grains and the initial porosity is large. In the heat treatment process, the unevenness of thermal expansion of mineral grains can be coordinated, to a certain extent, thus reducing the number of microcracks. At the same time, the change of sandstone cement after the high temperature is also beneficial, alleviating the effects of thermal cracking. However, in

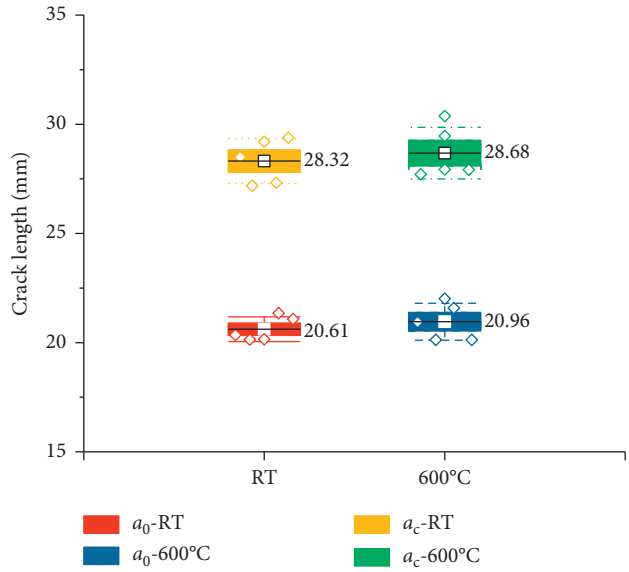

Figure 18: Initial crack length a_0 and critical effective crack length a_c.

crystalline rocks such as granite, the mineral grains are in close contact and the porosity is low. The uneven deformation of mineral grains caused by heat treatment cannot be coordinated, thermal stress is concentrated, and more thermal cracks appear. Therefore, the strength of crystalline rocks such as granite will be significantly reduced after being subjected to higher temperatures.

4.4. Changes of Clay Minerals after High Temperature. Water is an important factor affecting the strength of rocks [10]. There are many forms of water in rocks, including free water and bound water [51]. When the temperature exceeds 100°C, the free water gradually disappears, which will increase the effective stress (Sirdesai et al. [52]) and, at the same time, increase the friction between mineral grains, thereby increasing the strength of the rock (Zhang et al. [51]). When the temperature is further increased to above 400°C, the clay minerals begin to dehydrate, which also increases the friction between the mineral particles and is beneficial to increasing the rock strength [10].

When the temperature reaches 600°C, the kaolinite dehydroxylates to become metakaolinite, the activity is enhanced, the binding force between the mineral grains may be strengthened, and the mineral grains are bound more tightly [7, 36, 40], which all have a positive effect on increasing the ductility of the rock and its resistance to destruction. Ranjith et al. [7] also pointed out that the increase in ductility was related to the dehydroxylation of kaolinite in the Hawkesbury sandstone test after high-temperature treatment.

The XRD results (Figure 7) and thin section results (Figure 14) of this experiment indicate that the clay minerals of sandstone changed significantly after high-temperature treatment. This is a strengthening mechanism, which not only offsets the adverse effects of cracks caused by high temperatures on rock strength but even increases the resistance to the destruction of sandstone after high-temperature treatment; this strengthening mechanism is closely related to the change of clay minerals after high-temperature treatment.

During the heat treatment of rock, strengthening and weakening mechanisms coexist and compete with each other, which are closely related to various factors such as rock type, porosity, microstructure, water content, clay mineral content, and distribution. After the final heat treatment, the strength of the rock depends on the competition between the strengthening mechanism and the weakening mechanism. Undoubtedly, the competition process is complicated, and more detailed tests are needed for the in-depth analysis, which reflects the complexity of the physical and mechanical properties of rocks after high-temperature treatment.

4.5. Nonlinear Elastic Fracture Mechanics

$$\Delta a = a_c - a_0. \tag{15}$$

The average initial crack length a_0 of the SCB specimens at room temperature was 20.61 mm, and the average critical effective crack length a_c, calculated according to the double-K theory, was 28.32 mm. The critical effective crack growth was thus $\Delta a = 7.71$ mm (equation (15)), and so, $\Delta a/a_0 = 37.4\%$. The average crack length a_0 of the SCB specimens after high-temperature treatment at 600°C was 20.96 mm, and the average critical effective crack length a_c, calculated by the double-K theory, was 28.68 mm. The critical effective crack growth was thus $\Delta a = 7.72$ mm, and so, $\Delta a/a_0 = 36.8\%$, as shown in Figure 18.

It can be seen that the critical effective crack growth Δa of SCB specimens increased significantly at room temperature or after high-temperature treatment. This result is consistent with the experimental results of Miao et al. [18]. If the effective crack growth is not considered, the fracture

toughness value of the rock will be underestimated. The test results of many SCB specimens have also shown that the fracture toughness value is low [53]. Therefore, it is not appropriate to directly apply linear elastic fracture theory to analyze rocks.

5. Conclusions

As the mechanical properties of sandstone after treatment at high temperature are very important in the design and safety of many important projects, a variety of methods and techniques were used to test the mechanical properties, mineralogy, and microstructure of Sichuan sandstone at room temperature and after treatment at 600°C. Our conclusions are as follows:

(1) Compared with room temperature, there is no significant change in the strength and fracture toughness of Sichuan sandstone after 600°C, but the elastic modulus decreases

(2) After high-temperature treatment, the brittleness index (BI) of Sichuan sandstone decreases and the ductility increases. Both the stress-strain curve and the microscopic characteristics indicate that the brittleness of Sichuan sandstone decreases and the ductility increases after high-temperature treatment

(3) The clay minerals in the sandstone have significant changes after 600°C. For example, kaolinite is dehydroxylated to metakaolinite. This change may increase the ductility of the rock and have a positive effect on increasing the resistance of the rock to damage

(4) The mechanical properties of different types of rocks after high temperature are significantly different, which are not only related to the type of rock but also closely related to the mineral composition, the size and shape of mineral grains, and the distribution of microcracks and other microstructures

(5) Whether the Sichuan sandstone was treated at room temperature or 600°C, the unstable fracture toughness value obtained by the double-K theory was significantly greater than the apparent fracture toughness value. Considering the large critical effective crack growth Δa, linear elastic fracture theory should not be directly applied and it is more reasonable to use nonlinear elastic fracture theory

Data Availability

The data used to support the findings of this study are available from the corresponding author upon request.

Conflicts of Interest

The authors declare there are no conflicts of interest regarding the publication of this paper.

Authors' Contributions

J. L. performed the experiments and manuscript writing; Z. P. G. helped to analyze the results; Z. W. D. helped to perform the experiments and revised this manuscript.

Acknowledgments

This work was supported by the 2011 Collaborative Innovation Center for Green Development of Coal of Guizhou Province (Project No. [2016]02), Department of Education of Guizhou Province "125" Major Project ([2012]017), and the Joint Fund of Science and Technology Department of Guizhou Province (Project No. [2014]7457).

References

[1] J.-P. Zuo, J.-T. Wang, Y.-J. Sun, Y. Chen, G.-H. Jiang, and Y.-H. Li, "Effects of thermal treatment on fracture characteristics of granite from Beishan, a possible high-level radioactive waste disposal site in China," *Engineering Fracture Mechanics*, vol. 182, pp. 425–437, 2017.

[2] T. D. Rathnaweera, P. G. Ranjith, X. Gu et al., "Experimental investigation of thermomechanical behaviour of clay-rich sandstone at extreme temperatures followed by cooling treatments," *International Journal of Rock Mechanics and Mining Sciences*, vol. 107, pp. 208–223, 2018.

[3] P. K. Gautam, A. K. Verma, M. K. Jha, K. Sarkar, T. N. Singh, and R. K. Bajpai, "Study of strain rate and thermal damage of Dholpur sandstone at elevated temperature," *Rock Mechanics and Rock Engineering*, vol. 49, no. 9, pp. 3805–3815, 2016.

[4] L. Zhang, X. Mao, and A. Lu, "Experimental study on the mechanical properties of rocks at high temperature," *Science in China Series E: Technological Sciences*, vol. 52, no. 3, pp. 641–646, 2009.

[5] S. Liu and J. Xu, "An experimental study on the physico-mechanical properties of two post-high-temperature rocks," *Engineering Geology*, vol. 185, pp. 63–70, 2015.

[6] S.-Q. Yang, P. G. Ranjith, H.-W. Jing, W.-L. Tian, and Y. Ju, "An experimental investigation on thermal damage and failure mechanical behavior of granite after exposure to different high temperature treatments," *Geothermics*, vol. 65, pp. 180–197, 2017.

[7] P. G. Ranjith, D. R. Viete, B. J. Chen, and M. S. A. Perera, "Transformation plasticity and the effect of temperature on the mechanical behaviour of Hawkesbury sandstone at atmospheric pressure," *Engineering Geology*, vol. 151, pp. 120–127, 2012.

[8] P. Jin, Y. Hu, J. Shao, G. Zhao, X. Zhu, and C. Li, "Influence of different thermal cycling treatments on the physical, mechanical and transport properties of granite," *Geothermics*, vol. 78, pp. 118–128, 2019.

[9] N. N. Sirdesai, A. Singh, L. K. Sharma, R. Singh, and T. N. Singh, "Development of novel methods to predict the strength properties of thermally treated sandstone using statistical and soft-computing approach," *Neural Computing and Applications*, vol. 31, no. 7, pp. 2841–2867, 2019.

[10] L. N. Y. Wong, Y. Zhang, and Z. Wu, "Rock strengthening or weakening upon heating in the mild temperature range?" *Engineering Geology*, vol. 272, Article ID 105619, 2020.

[11] M. Ghamgosar and N. Erarslan, "Experimental and numerical studies on development of fracture process zone (FPZ) in

rocks under cyclic and static loadings," *Rock Mechanics and Rock Engineering*, vol. 49, no. 3, pp. 893–908, 2016.

[12] M. D. Kuruppu and M. Seto, *Determination of Fracture Toughness of Rock under In-Situ Conditions Using Semi-Circular Specimen*, ICF10, Honolulu, HI, USA, 2001.

[13] M. H. B. Nasseri, A. Schubnel, and R. P. Young, "Coupled evolutions of fracture toughness and elastic wave velocities at high crack density in thermally treated Westerly granite," *International Journal of Rock Mechanics and Mining Sciences*, vol. 44, no. 4, pp. 601–616, 2007.

[14] G. Feng, Y. Kang, T. Meng, Y.-Q. Hu, and X.-H. Li, "The influence of temperature on mode I fracture toughness and fracture characteristics of sandstone," *Rock Mechanics and Rock Engineering*, vol. 50, no. 8, pp. 2007–2019, 2017.

[15] M. Talukdar, D. Guha Roy, and T. N. Singh, "Correlating mode-I fracture toughness and mechanical properties of heat-treated crystalline rocks," *Journal of Rock Mechanics and Geotechnical Engineering*, vol. 10, no. 1, pp. 91–101, 2018.

[16] T. Yin, Q. Li, and X. Li, "Experimental investigation on mode I fracture characteristics of granite after cyclic heating and cooling treatments," *Engineering Fracture Mechanics*, vol. 222, Article ID 106740, 2019.

[17] G. Rong, J. Peng, M. Yao, Q. Jiang, and L. N. Y. Wong, "Effects of specimen size and thermal-damage on physical and mechanical behavior of a fine-grained marble," *Engineering Geology*, vol. 232, pp. 46–55, 2018.

[18] S. Miao, P. Z. Pan, P. Yu et al., "Fracture analysis of Beishan granite after high-temperature treatment using digital image correlation," *Engineering Fracture Mechanics*, vol. 225, Article ID 106847, 2019.

[19] V. Maruvanchery and E. Kim, "Effects of a high temperature (500°C) on the fracture processes in calcite-cemented sandstone along bedding-plane orientations," *Rock Mechanics and Rock Engineering*, vol. 53, no. 2, pp. 955–966, 2020.

[20] M. D. Kuruppu, Y. Obara, M. R. Ayatollahi, K. P. Chong, and T. Funatsu, "ISRM-suggested method for determining the mode I static fracture toughness using semi-circular bend specimen," *Rock Mechanics and Rock Engineering*, vol. 47, no. 1, pp. 267–274, 2014.

[21] S. Xu, M. A. Malik, Q. Li, and Y. Wu, "Determination of double-K fracture parameters using semi-circular bend test specimens," *Engineering Fracture Mechanics*, vol. 152, pp. 58–71, 2016.

[22] ISRM, "Suggested methods for determining tensile strength of rock materials," *International Journal of Rock Mechanics and Mining Sciences & Geomechanics Abstracts*, vol. 15, no. 3, pp. 99–103, 1978.

[23] G. Feng, X.-C. Wang, Y. Kang, S.-G. Luo, and Y.-Q. Hu, "Effects of temperature on the relationship between mode-I fracture toughness and tensile strength of rock," *Applied Sciences*, vol. 9, no. 7, p. 1326, 2019.

[24] T. Yin, Y. Wu, Q. Li, C. Wang, and B. Wu, "Determination of double-K fracture toughness parameters of thermally treated granite using notched semi-circular bending specimen," *Engineering Fracture Mechanics*, vol. 226, Article ID 106865, 2020.

[25] G. Ruiz, J. J. Ortega, R. C. Yu, S. Xu, and Y. Wu, "Effect of size and cohesive assumptions on the double-K fracture parameters of concrete," *Engineering Fracture Mechanics*, vol. 166, pp. 198–217, 2016.

[26] J.-P. Zuo, H.-P. Xie, F. Dai, and Y. Ju, "Three-point bending test investigation of the fracture behavior of siltstone after thermal treatment," *International Journal of Rock Mechanics and Mining Sciences*, vol. 70, pp. 133–143, 2014.

[27] G. V. Guinea, J. Y. Pastor, J. Planas, and M. Elices, "Stress intensity factor, compliance and CMOD for a general three-point-bend beam," *International Journal of Fracture*, vol. 89, no. 2, pp. 103–116, 1998.

[28] Systemes D, *ABAQUS/CAE 2016: Analysis User's Guide*, Dassault Systemes Simulia Corporation, Johnston, RI, USA, 2016.

[29] A. M. Pakdaman, M. Moosavi, and S. Mohammadi, "Experimental and numerical investigation into the methods of determination of mode I static fracture toughness of rocks," *Theoretical and Applied Fracture Mechanics*, vol. 100, pp. 154–170, 2019.

[30] J. Zuo, H. Xie, H. Zhou, and S. Peng, "Thermal-mechanical coupled effect on fracture mechanism and plastic characteristics of sandstone," *Science in China Series E: Technological Sciences*, vol. 50, no. 6, pp. 833–843, 2007.

[31] S. Chen, Z. Du, Z. Zhang, H. Zhang, Z. Xia, and F. Feng, "Effects of chloride on the early mechanical properties and microstructure of gangue-cemented paste backfill," *Construction and Building Materials*, vol. 235, Article ID 117504, 2020.

[32] S. Dong, L. Zeng, C. Xu et al., "A novel method for extracting information on pores from cast thin-section images," *Computers & Geosciences*, vol. 130, pp. 69–83, 2019.

[33] R. Guo, Q. Xie, X. Qu et al., "Fractal characteristics of pore-throat structure and permeability estimation of tight sandstone reservoirs: a case study of Chang 7 of the Upper Triassic Yanchang Formation in Longdong area, Ordos Basin, China," *Journal of Petroleum Science and Engineering*, vol. 184, Article ID 106555, 2020.

[34] Z. Li, "Effects of high temperatures on rocks," Doctoral thesis, Nanyang Technological University, Singapore, 2018.

[35] N. N. Sirdesai, B. Mahanta, P. G. Ranjith, and T. N. Singh, "Effects of thermal treatment on physico-morphological properties of Indian fine-grained sandstone," *Bulletin of Engineering Geology and the Environment*, vol. 78, no. 2, pp. 883–897, 2019.

[36] M. Hajpál and A. Török, "Mineralogical and colour changes of quartz sandstones by heat," *Environmental Geology*, vol. 46, no. 3-4, pp. 311–322, 2004.

[37] W. S. González-Gómez, P. Quintana, A. May-Pat, F. Avilés, J. May-Crespo, and J. J. Alvarado-Gil, "Thermal effects on the physical properties of limestones from the Yucatan Peninsula," *International Journal of Rock Mechanics and Mining Sciences*, vol. 75, pp. 182–189, 2015.

[38] Z. Li, L. N. Y. Wong, and C. I. Teh, "Low cost colorimetry for assessment of fire damage in rock," *Engineering Geology*, vol. 228, pp. 50–60, 2017.

[39] S. Sperinck, P. Raiteri, N. Marks, and K. Wright, "Dehydroxylation of kaolinite to metakaolin-a molecular dynamics study," *Journal of Materials Chemistry*, vol. 21, no. 7, pp. 2118–2125, 2011.

[40] B. Mahanta, P. G. Ranjith, V. Vishal, and T. N. Singh, "Temperature-induced deformational responses and microstructural alteration of sandstone," *Journal of Petroleum Science and Engineering*, vol. 192, Article ID 107239, 2020.

[41] M. Kataoka, S.-S. Jeong, Y. Obara, T. Yoshinaga, Y. Mine, and K. Takashima, "Testing method for determination of microscopic fracture toughness for rock materials," *Geotechnical Testing Journal*, vol. 41, no. 6, pp. 1092–1101, 2018.

[42] H. Su, H. Jing, M. Du et al., "Experimental investigation on tensile strength and its loading rate effect of sandstone after high temperature treatment," *Arabian Journal of Geosciences*, vol. 9, no. 13, p. 616, 2016.

[43] J. Peng, "Experimental study on the anisotropy and mode I fracture size effect of shallow marine sedimentary quartz sandstone," Doctoral Dissertation,University of Science and Technology Beijing, Beijing, China, 2018.
[44] V. J. García, C. O. Márquez, A. R. Zúñiga-Suárez, B. C. Zuñiga-Torres, and L. J. Villalta-Granda, "Brazilian test of concrete specimens subjected to different loading geometries: review and new insights," *International Journal of Concrete Structures and Materials*, vol. 11, no. 2, pp. 343–363, 2017.
[45] E. Komurlu, A. Kesimal, and S. Demir, "Experimental and numerical study on determination of indirect (splitting) tensile strength of rocks under various load apparatus," *Canadian Geotechnical Journal*, vol. 53, no. 2, pp. 360–372, 2016.
[46] B. Mahanta, T. N. Singh, and P. G. Ranjith, "Influence of thermal treatment on mode I fracture toughness of certain Indian rocks," *Engineering Geology*, vol. 210, pp. 103–114, 2016.
[47] D. Guha Roy, J. Singh, and M. Talukdar, "Correlating the mechanical and physical properties with mode-I fracture toughness of rocks," *Rock Mechanics and Rock Engineering*, vol. 50, no. 7, pp. 1941–1946, 2017.
[48] D. Zhang, P. G. Ranjith, M. S. A. Perera et al., "The brittleness indices used in rock mechanics and their application in shale hydraulic fracturing: a review," *Journal of Petroleum Science and Engineering*, vol. 143, pp. 158–170, 2016.
[49] T. Yin, X. Li, W. Cao, and K. Xia, "Effects of thermal treatment on tensile strength of Laurentian granite using Brazilian test," *Rock Mechanics and Rock Engineering*, vol. 48, no. 6, pp. 2213–2223, 2015.
[50] X. Liu, S. Yuan, Y. Sieffert, S. Fityus, and O. Buzzi, "Changes in mineralogy, microstructure, compressive strength and intrinsic permeability of two sedimentary rocks subjected to high-temperature heating," *Rock Mechanics and Rock Engineering*, vol. 49, no. 8, pp. 2985–2998, 2016.
[51] W. Zhang, Q. Sun, S. Hao, J. Geng, and C. Lv, "Experimental study on the variation of physical and mechanical properties of rock after high temperature treatment," *Applied Thermal Engineering*, vol. 98, pp. 1297–1304, 2016.
[52] N. N. Sirdesai, T. N. Singh, P. G. Ranjith, and R. Singh, "Effect of varied durations of thermal treatment on the tensile strength of red sandstone," *Rock Mechanics and Rock Engineering*, vol. 50, no. 1, pp. 205–213, 2017.
[53] T. Funatsu, N. Shimizu, M. Kuruppu, and K. Matsui, "Evaluation of mode I fracture toughness assisted by the numerical determination of K-resistance," *Rock Mechanics and Rock Engineering*, vol. 48, no. 1, pp. 143–157, 2015.